Antibacterial Surfaces Prepared Through Electropolymerization of *N*-Heterocyclic Carbene Complexes: a Pivotal Role of the Metal

Quentin Gaudillat,[1] Hamdi Ben Halima,[1] Agathe Figarol,[1] Vincent Humblot,[2] Isabelle Jourdain,[1] Boris Lakard,[1] Joan Bausells,[3] Lydie Viau[1] *

[1] Université Marie et Louis Pasteur, CNRS, Institut UTINAM (UMR 6213), F-25000 Besançon, France

[2] Université Marie et Louis Pasteur, CNRS, Institut FEMTO-ST (UMR 6174), F-25000 Besançon, France

[3] Institute of Microelectronics of Barcelona (IMB−CNM, CSIC), Campus UAB, 08193 Bellaterra, Barcelona, Spain

E-mail address: Lydie.viau@univ-fcomte.fr

ABSTRACT

N-heterocyclic carbene (NHC)-complexes are known to present antibacterial properties in solutions. However, these complexes have never been immobilized on solid supports to prepare antibacterial surfaces. Here, we tackled this lack and managed to immobilize these NHC-complexes on gold surfaces by electropolymerization. For this, we synthesized a series of various NHC complexes bearing different metals (M = Ag(I), Au(I), Rh(I), Ru(II), Cu(I)) and a pyrrole function. We measured the antibacterial properties of these complexes against two Gram-negative (*Escherichia coli* and *Pseudomonas aeruginosa)* and two Gram-positive bacteria (*Staphylococcus aureus* and *Listeria innocua*) by determination of their minimum inhibitory concentration (MIC) values. All NHC-complexes presented interesting antibacterial properties that are metal-dependent. The silver-NHC complex showed higher antibacterial activity against Gram-negative (MIC = 16 $\mu g.mL^{-1}$) than against Gram-positive bacteria (MIC = 32 $\mu g.mL^{-1}$) and was poorly efficient against *Listeria innocua.* All other metal-NHC complexes were more efficient against Gram-positive bacteria with MIC values in the range 4-16 $\mu g.mL^{-1}$. These NHC-complexes were then electropolymerized on gold substrates using their pyrrole function. Efficient incorporation of NHC-complexes into polypyrrole (PPy) films were confirmed by X-ray Photoelectron Spectroscopy (XPS) measurements with metal contents ranging from 0.8 % (Cu) to 12.3 % (Ag). Scanning Electron Microscopy (SEM) and profilometry measurements confirm that homogeneity, structure and thickness of the films depend on the metal. The antibacterial activities of the polypyrrole films were then determined by the halo inhibition method. We found a very good match between the antibacterial properties of the films and those of the monomers with Ag(I), Au(I) and Rh(I) complexes. With the other complexes, the metallic content was too low to obtain interesting antibacterial properties. The cytotoxicity of the films was finally evaluated on normal human dermal fibroblasts (NHDF). Our study reveals a strong impact of the doping anions of polypyrrole on the cell viability.

KEYWORDS:

N-Heterocyclic carbenes complexes, Gram-negative Bacteria, Gram-positive bacteria, antibacterial activities, electropolymerization, polypyrrole

1. INTRODUCTION

N-heterocyclic carbene (NHC) ligands possess the ability to bond as sigma donors to a wide range of hard and soft metals and can be readily functionalized. Thus, metal-NHC complexes have been used in several applications ranging from homogeneous catalysis to materials science.[1-3] Apart from their catalytical activity, metal-NHC complexes are also well known for their antibacterial activity. The first study on ruthenium and rhodium-NHC complexes showing antibacterial and antifungal properties was reported by Cetinkaya *et al*. in 1996.[4] Since then, numerous NHC-complexes have shown antibacterial properties, especially ruthenium(II),[5] silver(I),[6, 7] gold(I), [8, 9] and rhodium(I) ones.[10, 11] Most of these studied have focused on the measurements of the antibacterial activity of these complexes in solution. To our knowledge, they have never been immobilized on solid support to prepare antibacterial surfaces. Heterogenized metal NHC-complexes are, however, well known for catalytic applications.[12, 13] In this field, various supports have been used such as polystyrene,[14] silica,[15] polyoxometalate.[16] Besides the chemical grafting on a solid support, another strategy relied on the organic or inorganic chemical polymerization of metal-NHC complex monomers.[17-19] However, solubility problems always complicate thin films processing therefore direct formation of the polymer on the material to be coated is generally preferred. For this, the electropolymerization technic appears as a method of choice and presents many advantages such as easier surface modification, lower synthesis time and the possibility to control film thickness. In the literature, there are only a few examples on the electropolymerization of NHC-complexes. Cowley *et al.* reported in 2009 the first example of the electropolymerization of gold-NHC complexes containing pendant bithiophene moieties.[20] Later on, the same group described the electropolymerization of iridium and silver NHC complexes and studied the electrochromic properties of the resulting polythiophene films.[21] Other Ag(I), Cu(I) and Au(I)-NHC complexes with thiophene monomers were electropolymerized and used for electrochromic applications by Song *et al*.[22] while polythiophene films with Pd(II), Pt(II), Rh(I) and Ir(I) NHC- complexes were obtained by Jones *et al*.[23, 24] More recently, Kilinçarslan and collaborators studied the electropolymerization of Ru(II) and Pd(II)-NHC-complexes functionalized with carbazole.[25] Besides the study of the photophysical properties of the resulting metallo-polymers films, the electropolymerization of iron based *N*-heterocyclic carbene complexes bearing an 3,4-Ethylene dioxythiophene (EDOT) moiety has also been used to prepare functionalized electrodes for glucose sensing.[26] A pyrrole-functionalized ruthenium carbene complex was immobilized on an electrode surface through electropolymerization of the attached pyrrole and the resulting polypyrrole film was tested as heterogeneous catalyst in the epoxidation of various olefins.[27]

To our knowledge, the electropolymerization method has never been used to anchor metal-NHC complexes for antibacterial applications. Here, we electropolymerized a series of pyrrole-functionalized *N*-heterocyclic carbene complexes (M = Ag(I), Au(I), Rh(I), Ru(II), Cu(I)) on gold substrate to prepare antibacterial surfaces. We opted for these metals as NHC-complexes incorporating these metals are known for their antibacterial performances. Polypyrrole was chosen since this conducting polymer is considered biocompatible,[28-31] and is well known to present antibacterial properties against Gram-negative[32] and Gram-positive bacteria.[33, 34] Gold substrates were selected since gold implants have been used in various medical and dental fields.[35] The antibacterial properties of the NHC-complexes were first tested by determination of their minimal inhibitory concentration (MIC) against Gram-negative *Escherichia. coli* (*E. coli*) and *Pseudomonas aeruginosa* (*P. aeruginosa)* and against Gram-positive *Staphylococcus aureus* (*S. aureus*) and *Listeria innocua (L. innocua).* After electropolymerization, the antibacterial properties of the resulting films were tested against the same bacteria by means of agar diffusion tests and their cytotoxicity was evaluated on normal human dermal fibroblasts (NHDF).

2. MATERIALS AND METHODS

2.1. Materials and Chemicals

The chemicals used were obtained from the following commercial sources: pyrrole (99%) and NaH (60% dispersion mineral oil) from Acros Organics; 1,8- dibromooctane (98%) from Thermo Fischer, dichloro(*p*-cymene)ruthenium(II) dimer $[(RuCl_2(p\text{-cymene})]_2$ (98%) from Alfa-Aesar; *N*-methylimidazole (99%), acetonitrile (99.8%), toluene (99%), dichloromethane (99%) and methanol (99.5%) from Fischer ; silver oxide (Ag_2O) 99% from Thermo Scientific, chloro(dimethylsulfide)gold(I) ($AuCl(SMe_2)$) 97% from STREM ; chloro(1,5-cyclooctadiene)rhodium(I) dimer $[(Rh(cod)Cl)]_2$ was prepared from cyclooctadiene (97%) from Acros, and $RhCl_3.5H_2O$ from Aldrich according to a modified described procedure (no carbonate was added).[36] The culture media Mueller Hinton (MH) broth, Lysogeny broth Miller (Luria-Bertani), Brain Heart Infusion (BHI), Microbiology Agar, the cell medium (Dulbecco's modified Eagle's medium (DMEM), 2% glutamine), trypsin EDTA (0.25-0.002%), tryptan blue, fetal bovine medium were commercially obtained from Acros, Alfa Aesar, Merck, Fischer, Aldrich, TCI and Difco. The rectangular-gold substrates (10 mm × 10 mm) were prepared at IMB-CNB. Silicon wafers were covered by sputtering with 100 nm of silicon oxide,

then 50 nm Ti followed by 50 nm Ni and finally 200 nm layer of gold. The substrates were covered with a photoresist protection that was removed before experiments by washing with ethanol and ultrasound for 15 min. The resistivity range was about 4-40 Ω.cm.

2.2. Instrumentation

NMR. The ^{1}H and $^{13}C\{^{1}H\}$ NMR spectra were recorded on a Bruker AVANCE 400 HD instrument at 400 and 121.50 MHz respectively. Data are reported as chemical shifts in ppm, referenced to the proton impurity of the NMR solvent (^{1}H spectra) and to the NMR solvent ($^{13}C\{^{1}H\}$) spectra). When necessary, a combination of COSY, HSQC, HMBC was used to help assignment. Abbreviations used for the multiplicity in the ^{1}H NMR spectra are as follows: s, singlet; d, doublet; t: triplet; m: multiplet.

Infrared Spectra. A Bruker VERTEX 70 Fourier-Transform Infrared (FTIR) spectrometer equipped with an Attenuated Total Reflectance (ATR) unit was used to record the infrared spectra of the monomers (64 scans).

Water contact angles of the films were measured by the sessile drop technique using a GBX Scientific Instruments. One drop (1.5 µL) of distilled water was deposited on the sample surface with a syringe needle. Images were captured immediately after the deposition and were analyzed with Windrop software. Contact angles were determined by drawing the tangent close to the edge of the droplet. 5 measurements were performed for each sample.

Mechanical Profilometry. The thickness (T) was determined by profilometry using a mechanical probe profiler Dektak XT from Brüker (stylus size: 2.5 µm). Thicknesses were measured using a scan length of 5000 µm at a scan speed of 65 $\mu m \cdot s^{-1}$. Reported T values are the means of at least 5 measurements done at different places of the samples. For the measurements, a small stripe was made in the middle of the PPy films.

Scanning Electron Microscopy (SEM). The surface morphology of the films was obtained, without metallization treatment, using a high-resolution scanning electron microscope Apreo 2 from Thermo Scientific with an electron beam energy of 5 keV.

X-Ray Photoelectron Spectroscopy (XPS). Elemental and chemical structure analyses of the samples were performed using a Versaprobe 5000 spectrometer (ULVAC-PHI apparatus), utilizing a monochromatic and focused Al Kα X-ray source (hν = 1486.6 eV). For each sample, a survey spectrum and a high-resolution core level spectrum of C1s, N1s, O1s, F1s, P2p, Br3d,

Cl2p, I3d, Ag3d, Au4f, Rh3d, Ru3d, Cu2p levels, were recorded over a 200 µm spot size. The pass energies were 187.5 eV and 58.7 eV for the survey and core-level spectra, respectively. Data processing was performed using Casa XPS software and energy calibration was done on C1s C-C/C-H bonds at 284.8 eV.

High-resolution mass spectrometry (HRMS) measurements were performed at the Laboratoire de Mesures Physiques on a Synapt G2-S **(**Waters) equipped with an electrospray ionization source (ESI) and quadrupole-Time-of-Flight mass analyzer. The mass spectrometer was operated in the positive ion detection mode.

Elemental analyses were performed using a Thermoscientific FlashSmart (compounds weighed on a Satorius M2P, precision 10^{-6}g).

Electrochemistry. A SP-200 potentiostat from Biologic was used in all electrochemical experiments and the instrument was controlled by a PC computer via the EC-Lab V11.43 software interface. Electrochemical experiments were performed at room temperature (20°C) using a three-electrode setup with gold substrates (1 cm^2) as working electrodes, a Saturated Calomel Electrode (SCE) as a reference electrode and a platinum sheet as a counter-electrode. Polypyrrole films were obtained via cyclic voltammetry using acetonitrile solutions containing either 50 mM of the pyrrole monomer and 50 mM of the metal-NHC complexes or 100 mM of the pyrrole monomer + 100 mM tetrabutyl ammonium hexafluorophosphate ($TBAPF_6$) from +1.8 V/SCE to −0.6 V/SCE with a scan rate of 100 mV/s (8 cycles). The polypyrrole films are named according to the following: M-PPy where M = Ag, Au, Rh, Ru, Cu.

2.3.Antibacterial properties

Bacterial strains and growth conditions

Bacteria strains used in this work are Gram-negative *Escherichia coli (E. coli* ATCC 25922) and *Pseudomonas aeruginosa (P. aeruginosa* 01) and Gram-positive *Staphylococcus aureus* (*S. aureus* ATCC 25923) and *Listeria innocua* (*L. innocua Li2)* bacteria. All strains were stored at -80°C in culture media-glycerol aliquots. The inoculum was prepared first by growing a solid culture overnight at 30°C on Lysogeny Broth (Miller-LB, 20 $g.L^{-1}$) agar (15 $g.L^{-1}$) plate for *E. coli* and *P. aeruginosa,* at 37°C on Mueller-Hinton (MH, 25 $g.L^{-1}$) agar (15 $g.L^{-1}$) plate for *S. aureus* and at 37°C on Brain Heart Infusion (BHI, 37 $g.L^{-1}$) agar (15 $g.L^{-1}$) plate for *L. innocua*. Then, a liquid pre-culture was carried out by recovering one colony form the solid growth Petri

dishes on inoculated in 5 mL bacterial media at 30°C or 37°C, respectively overnight upon gentle stirring (90 rpm). Bacterial concentration in liquid culture was estimated to be close to 10^9 CFU.mL^{-1}via UV-Vis spectroscopy (UV-2450 Shimadzu spectrophotometer) at 620 nm using a calibration curve.

Minimal Inhibition Concentration (MIC) measurements

MIC values toward bacteria were determined by the 2-fold dilution method. Experiments were performed in 96-well microplates as triplicate in culture media (LB for *E. coli* and *P. aeruginosa*, MH for *S. aureus* and BHI for *L. innocua*). The initial bacterial concentration was approximately 10^6 CFU.mL^{-1}. The highest concentrations were prepared in distilled water. These concentrations were then two-fold serially diluted with broth. The 93-well microplates were then incubated overnight at 30°C/37°C. MICs correspond to the lowest concentration of the compound with no visible bacterial growth. The quality of the experiments was assessed by performing at the same time, sterility control (culture broth only), growth control (culture broth with bacteria), and death control (culture broth with bacteria and 50% ethanol) .

Inhibition zone assays

Polypyrrole films were placed face-down on *E. coli* or *P. aeruginosa* LB agar plates, *S. aureus* MH agar plates and *L. innocua* BHI agar plates previously incubated with a bacteria inoculum at a concentration of 10^6 colony forming units (CFU)/mL and then the plates were incubated at 30 or 37 °C overnight. Care should be taken to avoid any bubbles between the film and the agar. After overnight incubation, photos were recorded using an Interscience colony counter Scan 300.

Cell culture

NHDFs were purchased from Promocell (reference C-12302). Cells were cultured in Dulbecco's modified Eagle's medium (DMEM from Gibco, purity 100%) with 2% glutamine, complemented with 10% fetal bovine serum (FBS from Gibco purity 100%) and 1% penicillin-streptomycin from Sigma (10 000 U/mL penicillin, 10 000 µg/mL streptomycin), and incubated at 37 °C with 5% CO_2 in a humidified atmosphere. The cells were passaged every 3 or 4 days and seeded at 10 000 cells/cm^2 for culture maintenance.

Cytotoxicity Assays

For the assessment of cytotoxicity, the gold substrates covered with the **PPy** films were placed in a 24-well plate. In each well were added 60×10^3 cells in DMEM without SVF (1 mL/well). Controls and blanks were prepared by addition of cell media into empty wells with or without cells respectively. The cells were incubated for 24 h at 37 °C and 5% CO_2 before microscopic observations and cytotoxicity assays.

The assessment of cell necrosis was performed by measuring LDH (lactase dehydrogenase) release. The positive controls were prepared by addition of 10 µL Triton X-100 (From Genetec, purity 25%) in each well. The plate was then incubated for 30 min at 37 °C and 5% CO_2. 10 μL of the content in each well were removed and added to a new 24-well plate. To this new plate were added 100 μL of reactive mix according to the commercial protocol (Sigma-Aldrich MAK380 kit). After 30 min of incubation at room temperature protected from light, the absorbance was read at 450 nm (Clariostar plate reader). After removal of the absorbance of the blank, the results were expressed in percentage of the positive control.

The cell viability was evaluated using an MTT assay (Roche 11465007001 kit). In the first 24-well plate, we then removed 490 µL (remaining volume 500 µL) and added 10%v/v of MTT labeling agent (50 µL). The plate was then incubated for 4 hours at 37 °C and 5% CO_2. After this time, an equivalent volume (500 µL) of a HCl-propanol solution at 0.04M was added and the content of each well was gently stirred. The absorbance was then read at 570 nm. After removal of the absorbance of the blank, the results were expressed in percentage of the negative control (100% mitochondrial activity). Three independent experiments were carried out for each assay in triplicate. For statistical analysis, Fisher and Student's *t* tests were performed. The difference was declared to be significant when $p < 0.05$.

3. RESULTS AND DISCUSSION

3.1. Synthesis of the pyrrole-functionalized metal-NHC complexes

The synthesis route for the pyrrole-functionalized NHC-metal complexes (**Metal-NHCPy**) is outlined in Scheme 1. The brominated imidazolium [PyC_8MIm]Br was chosen as precursor and was synthesized according to our previous procedure.[37] Five complexes with different metals namely Ag(I), Au(I), Rh(I), Ru(II) and Cu(I) were prepared. The silver-NHC complex **Ag-NHCPy** was obtained from reaction of [PyC_8MIm]Br with silver(I) oxide in a vibratory ball-mill under solvent-free conditions according to a procedure described by Lamaty.[38] Under these

conditions, the reaction was finished within 10 minutes when performed in small scale (0.23 mmol) and within 1h30 when upscaled to 1.2 mmol. The **Ag-NHCPy** complex was obtained by simple filtration over a plug of celite in good yield (88%). Note that we failed to obtain the product when the reaction was performed using the solvent route. The four other metal-NHC complexes were obtained *via* transmetalation from the **Ag-NHCPy** complex.[39, 40] As mechanochemistry was efficient for the synthesis of the silver-NHC complex, we also tested these conditions for the transmetalation reactions. Unfortunately, only the **Ru-NHCPy** complex could be obtained by this method using $[RuCl_2(p\text{-cymene})]_2$ as the metal source. Nevertheless, the three other complexes **Au-NHCPy**, **Rh-NHCPy** and **Cu-NHCPy** were also obtained by transmetalation in good yields (76-98%) by the solvent route using the gold(I) precursor $AuCl(SMe_2)$, the rhodium(I) precursor $[Rh(cod)Cl]_2$, and CuI as Cu(I) source (see experimental details in the Supporting Information). The structure and the purity of the complexes were confirmed by ^{1}H and $^{13}C\{^{1}H\}$ NMR analyses, attenuated total reflection-infrared (ATR-IR) spectroscopy, and mass spectrometry (**Figures** S1−S15). Particularly, the formation of **Ag-NHCPy** was ascertained by the disappearance of the hydrogen of the imidazolium bromide at 10.7 ppm in its ^{1}H NMR spectrum. In the $^{13}C\{^{1}H\}$ NMR spectra, the signals of the C2 carbon were shifted downfield from 137.5 ppm for $[PyC_8MIm]Br$ to 181.4 ppm for **Ag-NHCPy**, 171.1 ppm for **Au-NHCPy**, 182.5 ppm for **Rh-NHCPy**, 173.5 ppm for **Ru-NHCPy** and 153.4 ppm for **Cu-NHCPy**. In the case of **Rh-NHCPy** this carbon appeared as a doublet due to presence of a $^{103}Rh–^{13}C$ coupling constant ($J_{C\text{-}Rh}$ = 51 Hz). All complexes were obtained as oils preventing their structural characterization by single-crystal X-Ray diffraction studies. **Ag-NHCPy** is not highly stable at room temperature in solution and was thus stored at 4°C in the dark and used for transmetallation reactions and electrochemical experiments just after being formed. **Cu-NHCPy** complex is also somehow labile and dissociates in solution to form the starting imidazolium bromide $[PyC_8MIm]Br$.

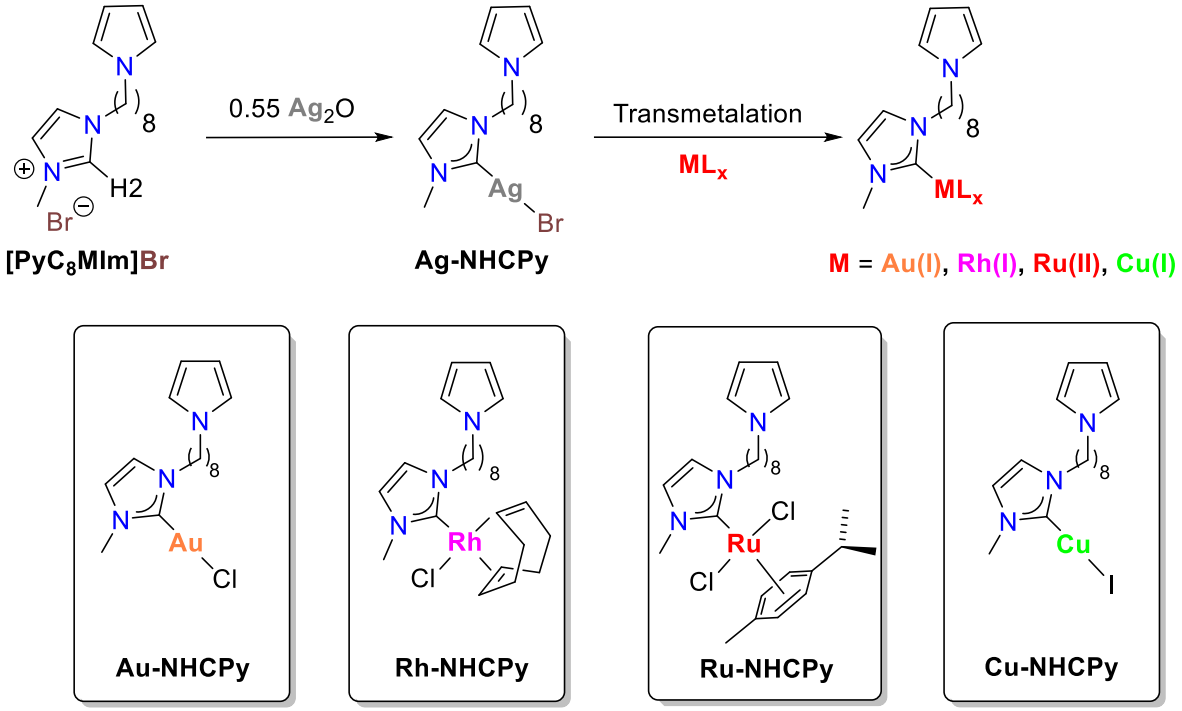

Reactant	Eq ML_x	Product	Conditions	Yield (%)
[PyC8MIm]Br	0.55 Ag_2O	**Ag-NHCPy**	vbm 25Hz 10 min	88
Ag-NHCPy	1.3 $AuCl(SMe_2)$	**Au-NHCPy**	CH_2Cl_2, RT, 24h	98
Ag-NHCPy	0.5 $[RhCl(cod)]_2$	**Rh-NHCPy**	CH_2Cl_2, reflux 24 h	95
Ag-NHCPy	0.5 $[RuCl_2(p\text{-cymene})]_2$	**Ru-NHCPy**	vbm, 29Hz, 1h40	96
Ag-NHCPy	1.1 CuI	**Cu-NHCPy**	CH_3CN, 60°C, 24h	76

Scheme 1. Conditions used for the synthesis of metal-NHCPy complexes.

3.2. Electrochemical deposition of polypyrrole films

The electrochemical oxidation of pyrrole (**Py**) and **M-NHCPy** monomers was performed using cyclic voltammetry from +1.8 V/SCE to -0.6 V/SCE on gold substrates at 100 mV/s using in all cases $TBAPF_6$ as electrolytes. The main advantages of the electrochemical technic rely on the fact that redox processes occurring during the film growth can be monitored *in situ* and films are directly deposited on the surface. The obtained cyclic voltammograms (CVs) are shown in Figure 1. A voltammogram of pyrrole performed in water solution usually contains two oxidation peaks and one reduction peak.[41] The oxidation peak at higher potential was attributed to the formation of pyrrole radical cations from pyrrole monomers by anodic oxidation, while the second oxidation peak corresponded to the oxidation of polypyrrole. The reduction peak was attributed to the reduction of polypyrrole. Usually, the intensity of the reduction and oxidation peaks of PPy increased with the number of cycle due to the formation

of more conducting PPy films while the intensity of the oxidation of the pyrrole monomer decreased due to the consumption of the reactant.[42] In acetonitrile solution, due to the low conductivity of the solution it has been shown that the oxidation peak of pyrrole was more difficult to observe.[43] All voltammograms of **M-NHCPy** except for **Ru-NHCPy** recorded in acetonitrile presented characteristic oxidation/reduction peaks of polypyrrole at +0.7V and 0V/SCE, respectively with current intensity that increased with cycles. In the case of **Ru-NHCPy** a decrease of the current with increasing cycles was observed due to the formation of less conductive PPy film rendering its electrochemical polymerization difficult.[44] In order to obtain several films for cell viability experiments (see section 3.5) we performed these electrodeposition experiments several times. We found our results to be reproducible and repeatable, films containing **Py**, **Ag-NHCPy**, **Au-NHCPy** and **Rh-NHCPy** could be easily obtained while it was difficult to polymerize **Ru-NHCPy**. In the case of **Cu-NHCPy**, the easy dissociation of the complex in solution (see discussion in section 3.1) rendered the experiment more difficult.

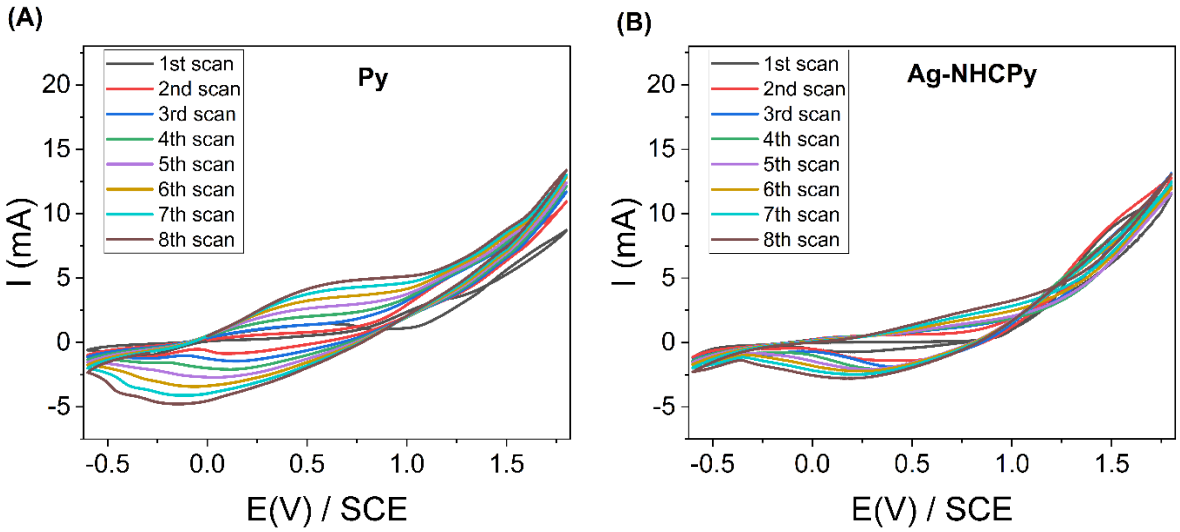

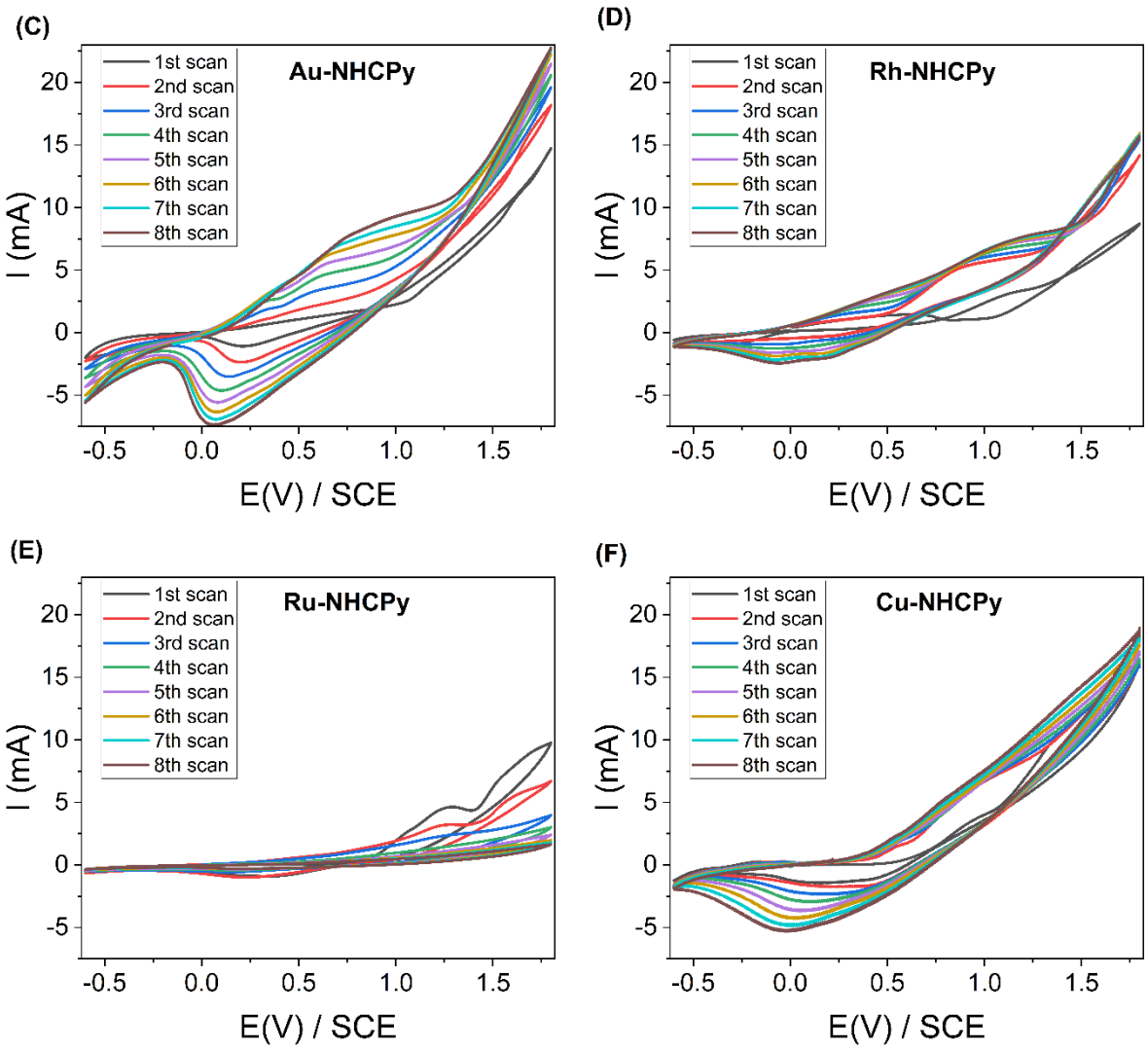

Figure 1. Potentiodynamic growth of polypyrrole films in acetonitrile solution containing 0.1 M $TBAPF_6$ with (A) 0.1 M pyrrole or (B)-(F) 0.05 M pyrrole + 0.05 M **M-NHCPy**.

3.3. Physico-chemical characterization of the films

It has been shown that antibacterial efficiency of polypyrrole is dependent to its morphology, especially particles' size.[45] We thus studied the morphological features of the films by Scanning Electron Microscopy (SEM). Films were named according to the metal used. All photographs presented in Figure 2 show a globular morphology characteristic of polypyrrole.[46] The size of their composing nodules was about 500 nm for **PPy** and **Au-PPy**, 400 nm **Cu-PPy** and 300 nm for **Ag-PPy**. **Rh-PPy** and **Ru-PPy** samples had a cauliflower-like morphology with larger aggregates.[47] The thicknesses of the electrodeposited films were measured by profilometry (Figure 2). Interestingly, films with the same morphology had thicknesses within the same range. Films with granular morphology were thicker (9.2 ± 0.4 µm for **PPy**, 10.7 ± 1.4 µm for

Ag-PPy, 11.2 ± 0.4 μm for **Au-PPy**, 7.5 ± 0.9 μm for **Cu-PPy**) while **Rh-PPy** and **Ru-PPy** with the larger aggregates were thinner (2.4 ± 0.5 and 2.0 ± 0.2 μm), respectively.

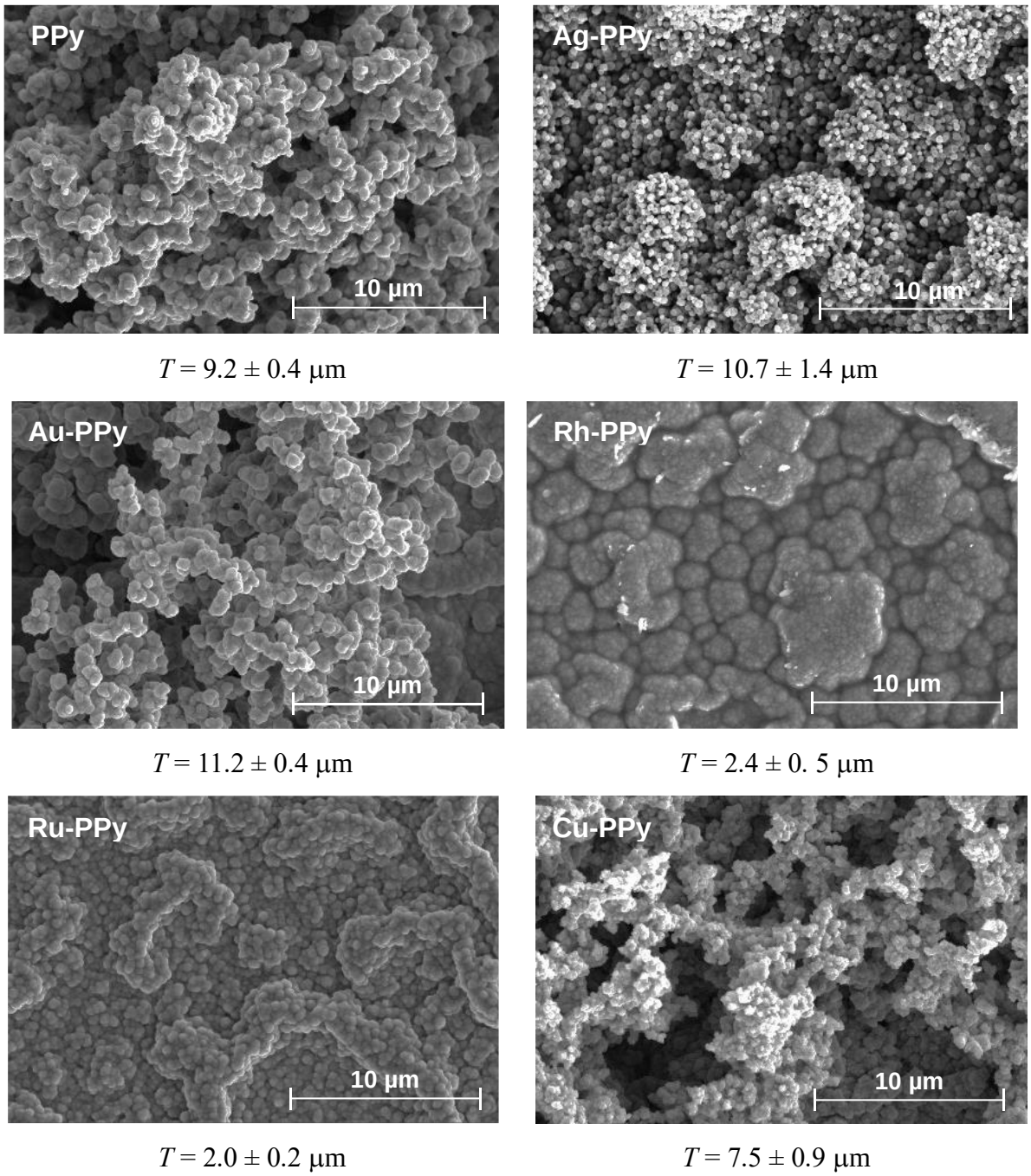

T = 9.2 ± 0.4 μm

T = 10.7 ± 1.4 μm

T = 11.2 ± 0.4 μm

T = 2.4 ± 0. 5 μm

T = 2.0 ± 0.2 μm

T = 7.5 ± 0.9 μm

Figure 2. SEM images of **PPy**, **M-PPy** (M = Ag, Au, Rh, Ru, Cu) films with their thickness *T*.

XPS analyses were further used to confirm the efficiency of the metal-NHC incorporation and the oxidation state of each metal. Table 1 summarizes the results of the survey and high-resolution spectra with the observed components, their binding energy and atomic percent. The

binding energies of the metal components and attributions are given in Table 2. C1s, N1s, P2p and F1S components were observed in all the films as expected from the formation of polypyrrole doped with PF_6^- anions. The presence of oxygen with an O1s peak at 531-532 eV might be attributed to the oxidation of polypyrrole during the electropolymerization process. This was confirmed by the presence of a band at low energy (398 eV) in the N1s spectra and bands at high energy in the C1s spectra.[48, 49] **M-PPy** films presented also Br3d/Cl2p/I3d and metal components (Ag3d, Au4f, Rh3d, Ru3d, Cu2p) confirming the incorporation of the carbene complexes (**Figures** S16-S21). The quantity of metal incorporated into the films varied with the nature of the metal and decreased in the order **Ag-PPy** (12.3%) > **Au-PPy** (5.1%) > **Rh-PPy** (2.6%) > **Ru-PPy** (4.5%) > **Cu-PPy** (0.8%). The high-resolution XPS spectrum of the Ag3d core-level peaks of **Ag-PPy** reported in Figure 3A presents one doublet fitted by a $3d_{5/2}$ (373.5 eV): $3d_{3/2}$ (367.5 eV) area ratio of 3:2.[50] The high-resolution Au4f XPS spectrum can be deconvolved into two main doublet signals (Figure 3B). The doublet with a binding energy of 85.0 eV (assigned as $Au4f_{7/2}$) and 88.6 eV (assigned as $Au4f_{5/2}$) can be ascribed to the Au(I) state, while the other set of signals at 83.9 and 87.5 eV were indexed to the presence of metallic gold. The voltammogram of **Au-NHCPy** did not show any peaks attributable to the reduction of Au(I) to Au(0) (Figure 1C). It has been reported that such a reduction occurred at -1 V/SCE, [51, 52] the potential used in this study was thus not low enough to reduce Au(I). The presence of Au(0) is therefore more likely due to the reduction of Au(I) during exposure of the film to the X-ray beam.[53] The survey of **Au-PPy** presented both Br3d and Cl2p components (ratio Cl/Br = 2.1) showing that the halogen exchange was not total (Figure S18). The Rh3d spectrum of **Rh-PPy** can be divided into two doublets peaks corresponding to Rh(I) (308.2 and 312.9 eV) and Rh(III) (310.0 and 314.87 eV) species in a 93:7 ratio indicating partial oxidation during electropolymerization (Figure 3C). This Rh(I)/Rh(III) oxidation was already observed during the electropolymerization of rhodium NHC-complexes featuring a terthiophene backbone.[24] As for **Au-PPy**, the presence of Br3d and Cl2p components (ratio Cl/Br = 6) indicated that some bromine remained in the monomer (Figure S19). For **Ru-PPy** a $Ru3d_{5/2}$ peak was clearly seen in the XPS spectrum at the lower energy side of the C1s peak (281.7 eV) (Figure 3D). The $Ru3d_{3/2}$ peak was observed at 285.9 eV (Δ = 4.8 eV) in accordance with literature values.[54, 55] This confirms that ruthenium was in +2 oxidation state in the film. The Cu2p XPS spectrum of **Cu-PPy** shows a spin-orbital doublet at binding energies of 932.8 eV and 952.6 eV attributed to $Cu2p_{3/2}$ and $Cu2p_{1/2}$, respectively (Figure 3E). There is no satellite structure of the Cu2p peak ruling out the presence of Cu^{2+} species.[56]

Table 1. XPS Data (binding energy (BE) and atomic %) for all **PPy** and **M-PPy** films.

Components BE (eV) /atom %	**PPy**	**Ag-PPy**	**Au-PPy**	**Rh-PPy**	**Ru-PPy**	**Cu-PPy**
C1s	284.8 68.5	284.8 54.4	284.8 68.6	284.8 72.7	284.8 74.8	284.8 73.4
N1s	399.8 10.7	400.8 9.5	400.7 13.9	400.1 10.0	400.8 5.6	400.1 13.7
O1s	532.0 6.0	531.5 8.9	532.2 0.9	531.5 10.9	532.9 1.4	531.1 4.0
F1s	686.2 12.4	686.4 3.1	686.3 7.8	686.0 2.0	686.1 10.5	686.2 5.0
P2p	135.9 2.4	136.1 0.6	136.3 1.2	136.2 0.4	136.1 1.7	136.5 0.8
Br3d	-	68.0 11.3	68.6 0.8	69.0 0.2	-	68.6 2.2
Cl2p	-	-	198.2 1.7	198.6 1.2	198.2 1.4	-
I3d	-	-	-	-	-	619.9 0.1
Metal	-	367.5 12.3	85.0 5.1	308.3 2.6	281.7 4.5	932.8 0.8

Table 2. Assignments of the metallic peaks present in all **M-PPy** spectra with binding energy (BE) in eV.

Sample	**Peak position (eV)**	**Peak attribution**	**Atom. %**

Ag-PPy	367.5 373.5	$3d_{5/2}$ Ag(I)X (3/5) $3d_{3/2}$ Ag(I)X (2/5)	60 40
Au-PPy	85.0 88.6	$4f_{7/2}$ Au(I)X (3/7) $4f_{5/2}$ Au(I)X (4/7)	37.0 27.8
	83.9 87.5	$4f_{7/2}$ Au(0) (3/7) $4f_{5/2}$ Au(0) (4/7)	20.1 15.1
Rh-PPy	308.2 312.9	$3d_{5/2}$ Rh(I)X (3/5) $3d_{3/2}$ Rh(I)X (2/5)	55.8 37.2
	310.0 314.8	$3d_{5/2}$ Rh(III)X (3/5) $3d_{3/2}$ Rh(III)X (2/5)	4.2 2.8
Ru-PPy	281.7 285.9	$3d_{5/2}$ Ru(II)X (3/5) $3d_{3/2}$ Ru(II)X (2/5)	60 40
Cu-PPy	932.8 952.6	2p3/2 Cu(I)X (2/3) 2p1/2 Cu(I)X (1/3)	66.6 33.3

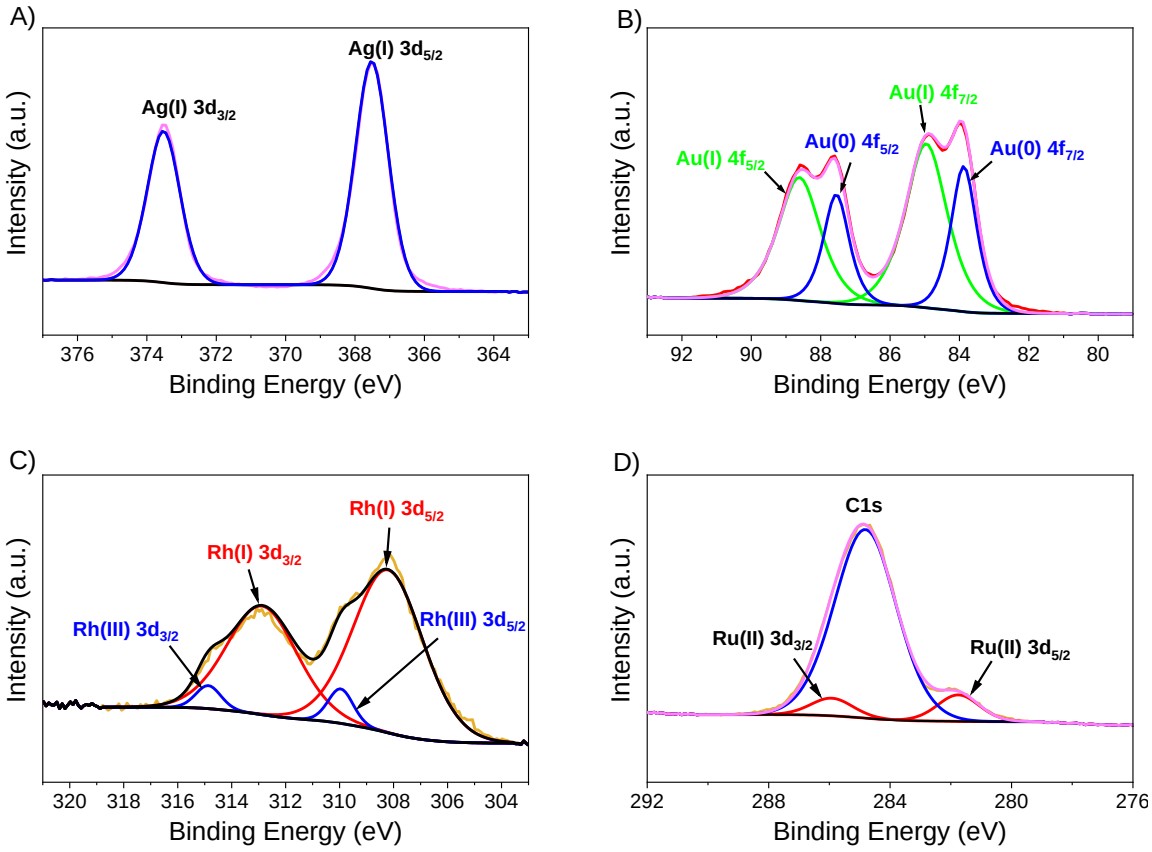

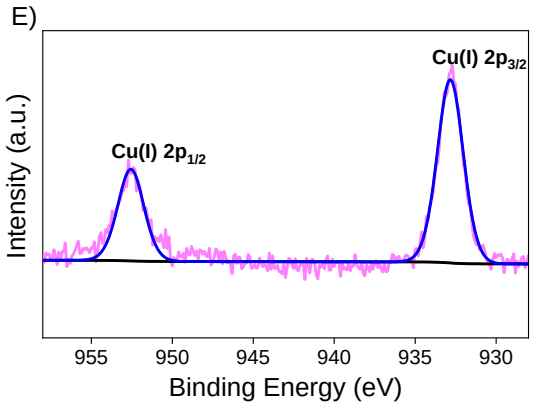

Figure 3. High resolution XPS spectra A) Ag3d of **Ag-PPy**, B) Au4f of **Au-PPy**, C) Rh3d of **Rh-PPy**, D) Ru3d of **Ru-PPy** and E) Cu2p of **Cu-PPy**.

3.4. Antibacterial properties

The i*n vitro* antimicrobial properties of the **Metal-NHCPy** monomers were first investigated by determination of their MICs against two Gram-negative bacteria (*E. coli* and *P. aeruginosa)* and two Gram-positive bacteria (*S. aureus and L. innocua)* (Table 3). For comparison, the results obtained with [PyC$_8$MIm]Br are also given in Table 4. The imidazolium salt **[PyC$_8$MIm]Br** showed only a low activity against *S. aureus* with a MIC value of 128 µg.mL^{-1}. All **M-NHCPy** complexes presented stronger antibacterial activity against all strains. **Ag-NHCPy** was more active against Gram- than Gram+ bacteria with MICs of 16 µg.mL^{-1} against *E. coli* and *P. aeruginosa*. These values are within the range found for other NHC-AgBr complexes (Table 4).[7] The activity of **Au-NHCPy** against Gram- was very similar to **Ag-NHCPy** but it possessed much better activity against Gram+ bacteria (MICs = 4-8 µg.mL^{-1}). A better efficiency of Au-NHC complexes against Gram+ bacteria was also observed by Ott and collaborators.[57] **Rh-NHCPy** had no activity against Gram- bacteria but good ones against Gram+ bacteria with the best against *S. aureus* (MIC = 4 µg.mL^{-1}). **Ru-NHCPy** showed moderate or low activity against especially Gram- bacteria but good activity against Gram+ (MIC = 16 µg.mL^{-1}) in accordance with previous results.[58, 59] **Cu-NHCPy** behaved almost like **Au-NHCPy** with good activity against all bacteria strains but more efficiency against Gram+ bacteria (MICs = 4-8 µg.mL^{-1}) as observed by Pan and collaborators for various Cu-NHC complexes.[60]

Table 3. Comparison of MIC values for the **M-NHCPy** monomers (in µg.mL^{-1}).

Compounds	Gram-negative		Gram-positive		reference
	E. coli	*P .aeruginosa*	*S. aureus*	*L. innocua*	
[PyC$_8$MIm]Br	> 512	> 512	128	> 512	
Ag-NHCPy	16	16	32	256	This work
Ag-NHCBr	*200*	*200*	*200*		[61]
	5.85-44.4		*5.85-19.75*		[62]
			25		[63]
	6.25-100	*6.25-100*	*6.25-50*		[64]
Au-NHCPy	16	32	8	4	This work
Au-NHCCl	*13-45*	*>50*	*0.28-3.2*		[57]
Rh-NHCPy	> 512	> 512	4	16	This work
Ru-NHCPy	64	128	16	16	This work
Ru-NHC(p-cymene)Cl$_2$	*25-50*		*25*		[58]
Cu-NHCPy	32	32	4	8	This work

We then evaluated qualitatively the antibacterial properties of the films by inhibition zone assays using the same bacteria strains. For this, the substrates with the films were placed in Petri dishes containing gel culture medium inoculated with 10^6 CFU.mL^{-1} bacteria. All films were highly opaque, making it difficult to observe bacteria. This is the reason why we focused solely on the presence or absence of an inhibition halo around the films. Results were considered positive (noted +) if a halo of inhibition was clearly visible and very positive in the case of the presence of large halo (++). If a faint halo was observed, results were marked (+-) while in the absence of halo, the result was considered negative (-). Figure 4 shows the images of the films after 24 hours incubation and the halos are indicated by a white circle. The table in Figure 4 summarizes the results. MICs values of the monomers were also included for a better comparison. First, as can be seen in Figure 4, **PPy** did not present any halo on agar plates containing all bacteria. **PPy-Ag** films had halos in the presence of all bacteria except *L. innocua,* in accordance with the results obtained with the silver NHC monomer. For **PPy-Au**, antibacterial activities were observed for all bacteria. The size of the halos was nevertheless

smaller than for **Ag-PPy** films. The halos for **Cu-PPy** were relatively small despite the good antibacterial activity of its monomer because the quantity of the monomer incorporated in the film was very small (0.8 atom. %). **Rh-PPy** films presented halos only in contact with Gram- bacteria as expected from the antibacterial property of **Rh-NHCPy**. Thus, with these results we have shown a good relationship between the inhibition zone assays of the films and the antibacterial properties of the monomers. The only exception was obtained with **Ru-PPy** films that did not possess any halos despite the relatively good activity of the monomer and a metal atomic content of 4.5%. The low activity was most probably due to the fact that despite a relatively high ruthenium content determined on the surface by XPS, the quantity of metal incorporated into the whole film was lower than for the other samples as the film was much thinner.

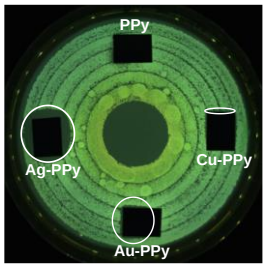

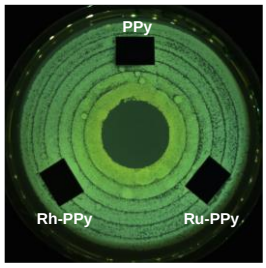

E. coli

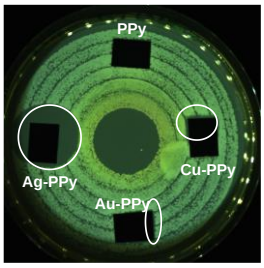

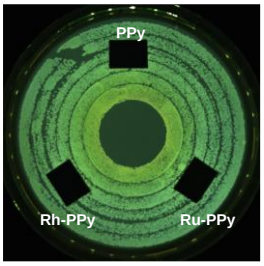

P. aeruginosa

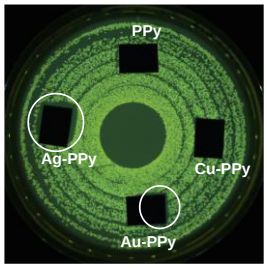

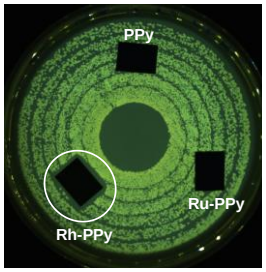

S. aureus

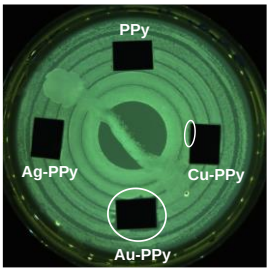

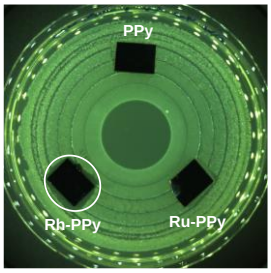

L. innocua

Films	Bacteria							
	Gram -				Gram +			
	E. coli	MIC[a]	*P. aeruginosa*	MIC[a]	*S. aureus*	MIC[a]	*L. innocua*	MIC[a]
PPy	-		-		-		-	
Ag-PPy	++	16	++	16	+	32	-	256
Au-PPy	+	16	+	32	+	8	++	4
Rh-PPy	-	> 512	-	> 512	++	4	+	16
Ru-PPy	-	64	-	128	-	16	-	16
Cu-PPy	+-	32	+	32	-	4	+-	8

Figure 4. Comparison of inhibition zone assays obtained with **PPy** and **Metal-PPy** films against Gram-Positive and Gram-Negative Bacteria. [a] MIC values of the monomers in µg.mL^{-1}.

After this first series of experiments, all films were rinsed with ethanol and then re-subjected to the contact test protocol. In this case, only the **Ag-PPy** film still demonstrated antibacterial properties (Figure S22).

3.5. Cytotoxicity measurements

The *in vitro* cytotoxicity of the films was tested on human dermal fibroblasts by MTT (3-(4,5-dimethylthiazol-2-yl)-2,5-diphenyltetrazolium bromide) assays. Cells were incubated overnight at 37°C with all different films. The results reported in Figure 5A show that all **M-PPy** films were cytotoxic with cell viability below 80%. Surprisingly, even the **PPy** film was found to be cytotoxic despite several studies having evidenced its biocompatiblility.[28, 65] In these studies, the positively charged **PPy** contained chloride anions. Thus, the hexafluorophoshate anions used in our case were probably responsible for the observed cytotoxicity of our films. To verify this hypothesis, we also prepared a **PPy** film using lithium bis(trifluoromethylsulfonyl)imide as electrolyte. In this case, cell viability reached 74% confirming the strong influence of the doping anion on the cytotoxicity. **Ag-PPy** and **Cu-PPy** films presented the lowest cell viability of 19% that might be linked to the low stability of the NHC-complexes. This chemical instability might lead to the release of Ag^+ ions and Cu^+ ions that are quickly oxidized under ambient conditions to Cu^{2+} ions. These Cu^{2+} ions are known to form reactive oxygen species.[66] **Ru-PPy** also presented a relatively high cytotoxicity with 34% cell viability after 24 hours. As mentioned before, the presence of PF_6^- anions might be responsible for this. To prove this hypothesis, we determined the doping level of the polymer using the N/F ratio measured by XPS[67] (See Table in Figure 5). For **Ru-PPy**, the N/F ratio was very low (0.5) meaning that the amount of PF_6^- incorporated was very important. In fact, the doping level of **Ru-PPy** was very close to the one of **PPy** (0.9). For **Ag-PPy** and **Cu-PPy** the doping level was low (high N/F ratio) confirming that the release of metal ions was most probably responsible for their cytotoxicity. Less cytotoxic films were **Au-PPy** and **Rh-PPy** that did not incorporate a high content of PF_6^- anions (N/F ratio of 1.8 and 5.0, respectively). The loss of membrane integrity was then evaluated by released lactate dehydrogenase (LDH) quantification. LDH is a cytoplasmic soluble enzyme, which is quickly released into the extracellular medium due to cell membrane damage. The LDH release led to a cascade of reactions that finally transformed INT (2-(4-iodophenyl)-3-(4-nitrophenyl)-5-phenyl-2*H*-

tertrazolium) added to the medium to red formazan whose formation can be spectrophotometrically quantified at 450 nm.[68] In the case of **PPy** ($TBAPF_6$) and **Au-PPy**, the decrease of cell viability was mainly due to necrosis (55 %) while for the other films apoptosis was responsible for cell death. This is in line with the mode of action usually observed for metal complexes[69] and carbenes derivatives[70, 71]

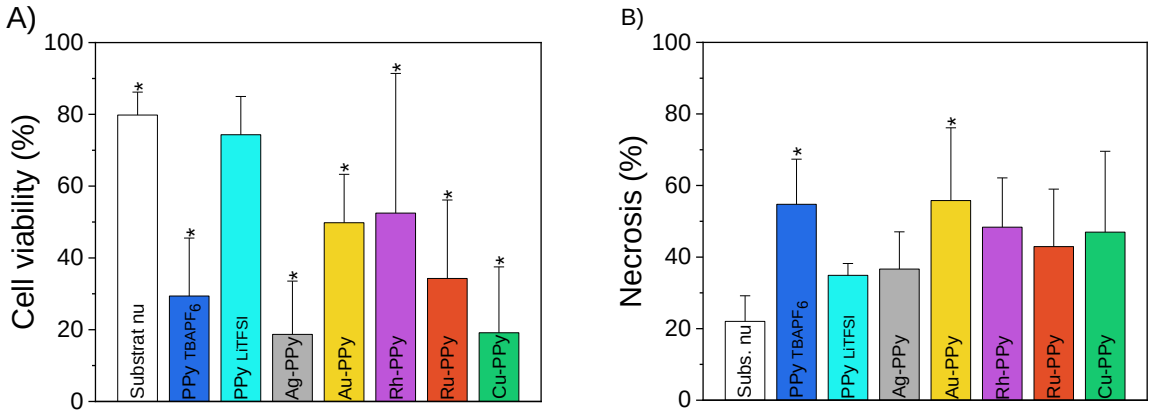

	Cell viability (%)	N/F[a]	Metal content (%)[a]
PPy ($TBAPF_6$)	29±15	0.9	-
PPy (LiTFSI)	74±10		
Ag-PPy	19±15	3.1	12.3
Au-PPy	49±13	1.8	5.1
Rh-PPy	52±39	5.0	2.6
Ru-PPy	34±15	0.5	4.5
Cu-PPy	19±18	2.7	0.8

[a] measured by XPS.

Figure 5. Cytotoxicity of **PPy** and **M-PPy** films on human dermal fibroblasts (*P<0.05) detected by A) MTT assay and B) LDH release.

4. Conclusions

N-Heterocyclic carbene complexes with various metals (Ag(I), Au(I), Rh(I), Ru(II), and Cu(I)) and functionalized with a pyrrole group were synthesized by traditional solvent route and, when possible, using mechanochemistry. Investigation of the antibacterial properties by MIC

determination showed good antibacterial efficiency against two strains of Gram-positive and Gram-negative bacteria for all these electroactive monomers. More interestingly, we found that antibacterial properties were metal-dependent. All complexes, except the silver-one, were more active against Gram-positive bacteria.

We then report for the first time the elaboration of antibacterial surfaces prepared by electropolymerization of these NHC-complexes on gold surface. The physicochemical characterization evidenced that in the case of copper and ruthenium, the films were not of sufficient quality to offer any interesting antibacterial activity. Indeed, the copper NHC complex was not stable enough to allow a high amount of copper incorporation into the film. In the case of the ruthenium complex, its electrochemical polymerization was difficult leading to the formation of poorly conductive thin film. However, the electropolymerization of the other NHC complexes (Ag(I), Au(I), Rh(I)) went smoothly and led to homogeneous films with metal contents varying from 2.6 to 12.3 atomic percents. These films presented interesting antibacterial properties with a dependency on the nature of the bacteria in line with that of the monomers. The film containing Au(I) was active against all bacteria strains while the one incorporating the rhodium complex was only efficient against Gram-positive bacteria. The polypyrrole film formed with the silver complex was active against all bacteria except *Listeria innocua*. Unfortunately, we found that all films presented cytotoxicity towards normal human dermal fibroblasts. However, preliminary encouraging results have shown that the most probable reason for this cytotoxicity was due to the electrolyte salt used for electropolymerization. Our preliminary result succeeded in demonstrating that a simple modification of the nature of the doping anions led to a drastic decrease in cytotoxicity. We are now pushing forwards this study concentrating on the most promising Ag, Au and Rh NHC-complexes to elaborate non-cytotoxic antibacterial films. For this, an interesting strategy will be to used pharmaceutically active ingredients.[44]

Data availability

ASSOCIATED CONTENT

Supporting Information. Additional experimental details, ^{1}H and $^{13}C\{^{1}H\}$ NMR spectra of all complexes, Infra-Red spectra for all complexes, survey XPS spectra for all films, images of the PPy films upon exposure for a second time after rinsing with ethanol to Gram-positive and Gram-negative bacteria (PDF). The following files are available free of charge on the ACS publication website at http://pubs.acs.org.

Author information

* E-mail: lydie.viau@univ-fcomte.fr

Author Contributions

The manuscript was written through contributions of all authors. All authors have given approval to the final version of the manuscript.

Funding

This research was funded by the Regional Council of Bourgogne Franche-Comté through the Envergure Program MatElectroCap. This work has been achieved in the frame of the EIPHI Graduate school (contract "ANR-17-EURE-0002").

Notes

The authors declare no competing financial interest.

ACKNOWLEDGEMENTS

Q.G. thanks the Ministère de l'Enseignement Supérieur et de la Recherche for his PhD scholarship. We indebted to S. Adache from SynBioN (Université de Lorraine-CNRS – http://synbion.univ-lorraine.fr/accueil/) for the elemental analyses. Anna Krystianiak from the ARCEN-Carnot platform (ICB) is gratefully acknowledged for carrying out the XPS analyses. We are also thankful to Stéphanie Beffy from the Plateforme Chimie UTINAM for her help with NMR measurements.

REFERENCES

1. Nahra, F.; Cazin, C. S. J., Sustainability in Ru- and Pd-Based Catalytic Systems Using *N*-Heterocyclic Carbenes as Ligands. *Chem. Soc. Rev.* **2021,** *50* (5), 3094-3142.

2. Mercs, L.; Albrecht, M., Beyond Catalysis: *N*-Heterocyclic Carbene Complexes as Components for Medicinal, Luminescent, and Functional Materials Applications. *Chem. Soc. Rev.* **2010,** *39* (6), 1903-1912.

3. He, R.; Xu, Z.; Valandro, S.; Arman, H. D.; Xue, J.; Schanze, K. S., High-Purity and Saturated Deep-Blue Luminescence from trans-NHC Platinum(II) Butadiyne Complexes: Properties and Organic Light Emitting Diode Application. *ACS Appl. Mater. Interfaces* **2021,** *13* (4), 5327-5337.

4. Cetinkaya, B.; Cetinkaya, E.; Küçükbay, H.; Durmaz, R., Antimicrobial Activity of Carbene Complexes of Rhodium(I) and Ruthenium(II). *Arzneim.-Forsch.* **1996,** *46* (8), 821-3.

5. Catalano, A.; Mariconda, A.; Sinicropi, M. S.; Ceramella, J.; Iacopetta, D.; Saturnino, C.; Longo, P., Biological Activities of Ruthenium NHC Complexes: An Update. *Antibiotics* **2023,** *12* (2), 365.

6. Ronga, L.; Varcamonti, M.; Tesauro, D., Structure–Activity Relationships in NHC–Silver Complexes as Antimicrobial Agents. *Molecules* **2023,** *28* (11), 4435.

7. Isbel, S. R.; Patil, S. A.; Bugarin, A., NHCs Silver Complexes as Potential Antimicrobial Agents. *Inorg. Chim. Acta* **2024,** *563*, 121899.

8. Mora, M.; Gimeno, M. C.; Visbal, R., Recent Advances in Gold–NHC Complexes with Biological Properties. *Chem. Soc. Rev.* **2019,** *48* (2), 447-462.

9. Ratia, C.; Soengas, R. G.; Soto, S. M., Gold-Derived Molecules as New Antimicrobial Agents. *Front. Microbiol.* **2022,** *13*.

10. Hindi, K. M.; Panzner, M. J.; Tessier, C. A.; Cannon, C. L.; Youngs, W. J., The Medicinal Applications of Imidazolium Carbene−Metal Complexes. *Chem. Rev.* **2009,** *109* (8), 3859-3884.

11. Oehninger, L.; Rubbiani, R.; Ott, I., N-Heterocyclic Carbene Metal Complexes in Medicinal Chemistry. *Dalton Trans.* **2013,** *42* (10), 3269-3284.

12. Cazin, C. S. J., Recent Advances in the Design and Use of Immobilised N-Heterocyclic Carbene Ligands for Transition-Metal Catalysis. *C. R. Chim.* **2009,** *12* (10-11), 1173-1180.

13. Sommer, W. J.; Weck, M., Supported N-Heterocyclic Carbene Complexes in Catalysis. *Coord. Chem. Rev.* **2007,** *251* (5), 860-873.

14. Kim, J.-H.; Kim, J.-W.; Shokouhimehr, M.; Lee, Y.-S., Polymer-Supported N-Heterocyclic Carbene−Palladium Complex for Heterogeneous Suzuki Cross-Coupling Reaction. *J. Org. Chem.* **2005,** *70* (17), 6714-6720.

15. Corma, A.; Gutiérrez-Puebla, E.; Iglesias, M.; Monge, A.; Pérez-Ferreras, S.; Sánchez, F., New Heterogenized Gold(I)-Heterocyclic Carbene Complexes as Reusable Catalysts in Hydrogenation and Cross-Coupling Reactions. *Adv. Synth. Catal.* **2006,** *348* (14), 1899-1907.
16. Modugno, G.; Monney, A.; Bonchio, M.; Albrecht, M.; Carraro, M., Transfer Hydrogenation Catalysis by a N-Heterocyclic Carbene Iridium Complex on a Polyoxometalate Platform. *Eur. J. Inorg. Chem.* **2014,** *2014* (14), 2356-2360.
17. Wei, Z.; Kayceety, M.; Price, A.; Wei, K.; Luo, Q.; Thanneeru, S.; Sun, S.; He, J., Polymer N-Heterocyclic Carbene (NHC) Ligands for Silver Nanoparticles. *ACS Appl. Mater. Interfaces* **2022,** *14* (49), 55227-55237.
18. MacLeod, M. J.; Johnson, J. A., PEGylated N-Heterocyclic Carbene Anchors Designed To Stabilize Gold Nanoparticles in Biologically Relevant Media. *J. Am. Chem. Soc.* **2015,** *137* (25), 7974-7977.
19. Ferré, M.; Cattoën, X.; Wong Chi Man, M.; Pleixats, R., Sol–Gel Immobilized N-Heterocyclic Carbene Gold Complex as a Recyclable Catalyst for the Rearrangement of Allylic Esters and the Cycloisomerization of γ-Alkynoic Acids. *ChemCatChem* **2016,** *8* (17), 2824-2831.
20. Powell, A. B.; Bielawski, C. W.; Cowley, A. H., Electropolymerization of an N-Heterocyclic Carbene−Gold(I) Complex. *J. Am. Chem. Soc.* **2009,** *131* (51), 18232-18233.
21. Powell, A. B.; Bielawski, C. W.; Cowley, A. H., Design, Synthesis, and Study of Main Chain Poly(N-Heterocyclic Carbene) Complexes: Applications in Electrochromic Devices. *J. Am. Chem. Soc.* **2010,** *132* (29), 10184-10194.
22. Satheeshkumar, C.; Park, J.-Y.; Jeong, D.-C.; Song, S. G.; Lee, J.; Song, C., Synthesis and Electronic Properties of N-Heterocyclic Carbene-Containing Conducting Polymers with Coinage Metals. *RSC Adv.* **2015,** *5* (75), 60892-60897.
23. Wang, W.; Guo, H.; Jones, R. A., Synthesis and Electropolymerization of N-Heterocyclic Carbene Complexes of Pd(ii) and Pt(ii) from an Emissive Imidazolium Salt with a Terthiophene Backbone. *Dalton Trans.* **2019,** *48* (38), 14440-14449.
24. Wang, W.; Lynch, V. M.; Guo, H.; Datta, A.; Jones, R. A., Electropolymerizable *N*-Heterocyclic Carbene Complexes of Rh and Ir with Enantiotropic Polymorphic Phases. *Dalton Trans.* **2020,** *49* (7), 2264-2272.
25. Karakaş, H.; Güzel, M.; Ak, M.; Kılınçarslan, R.; Özdemir, N., N,S-heterocyclic carbene containing benzothiazol-2-ylidene-Ru(II) and Pd(II) new complexes functionalized

with butyl linked carbazole moiety: Synthesis, characterization and their catalytic efficiency and electropolymerizations. *Eur. Polym. J.* **2022,** *181*, 111630.

26. Cingolani, A.; Olivieri, D.; Messori, A.; Cesari, C.; Zanotti, V.; Zacchini, S.; Gualandi, I.; Scavetta, E.; Mariani, F.; Tonelli, D.; Mazzoni, R., Electrochemical polymerisation of newly synthesised 3,4-ethylene dioxythiophene-N-heterocyclic carbene iron complexes and application as redox mediators. *Inorg. Chim. Acta* **2022,** *542*, 121138.

27. Dakkach, M.; Fontrodona, X.; Parella, T.; Atlamsani, A.; Romero, I.; Rodríguez, M., Polypyrrole-Functionalized Ruthenium Carbene Catalysts as Efficient Heterogeneous Systems for Olefin Epoxidation. *Dalton Trans.* **2014,** *43* (26), 9916-9923.

28. Wang, X.; Gu, X.; Yuan, C.; Chen, S.; Zhang, P.; Zhang, T.; Yao, J.; Chen, F.; Chen, G., Evaluation of Biocompatibility of Polypyrrole In Vitro and In Vivo. *J. Biomed. Mater. Res.* **2004,** *68A* (3), 411-422.

29. Aufan, M. R.; Sumi, Y.; Kim, S.; Lee, J. Y., Facile Synthesis of Conductive Polypyrrole Wrinkle Topographies on Polydimethylsiloxane via a Swelling–Deswelling Process and Their Potential Uses in Tissue Engineering. *ACS Appl. Mater. Interfaces* **2015,** *7* (42), 23454-23463.

30. Kim, S.; Jang, L. K.; Jang, M.; Lee, S.; Hardy, J. G.; Lee, J. Y., Electrically Conductive Polydopamine–Polypyrrole as High Performance Biomaterials for Cell Stimulation in Vitro and Electrical Signal Recording in Vivo. *ACS Appl. Mater. Interfaces* **2018,** *10* (39), 33032-33042.

31. Alegret, N.; Dominguez-Alfaro, A.; González-Domínguez, J. M.; Arnaiz, B.; Cossío, U.; Bosi, S.; Vázquez, E.; Ramos-Cabrer, P.; Mecerreyes, D.; Prato, M., Three-Dimensional Conductive Scaffolds as Neural Prostheses Based on Carbon Nanotubes and Polypyrrole. *ACS Appl. Mater. Interfaces* **2018,** *10* (50), 43904-43914.

32. Varesano, A.; Aluigi, A.; Florio, L.; Fabris, R., Multifunctional Cotton Fabrics. *Synth. Met.* **2009,** *159* (11), 1082-1089.

33. Varesano, A.; Vineis, C.; Tonetti, C.; Mazzuchetti, G.; Bobba, V., Antibacterial Property on Gram-Positive Bacteria of Polypyrrole-Coated Fabrics. *J. Appl. Polym. Sci.* **2015,** *132* (12).

34. Marestoni, L. D.; Barud, H. d. S.; Gomes, R. J.; Catarino, R. P. F.; Hata, N. N. Y.; Ressutte, J. B.; Spinosa, W. A., Commercial and Potential Applications of Bacterial Cellulose in Brazil: Ten Years Review. *Polímeros* **2020,** *30*.

35. Demann, E. T. K.; Stein, P. S.; Haubenreich, J. E., Gold as an Implant in Medicine and Dentistry. **2005,** *15* (6), 687-698.

36. G. Giordano, R.H. Crabtree, R.M. Heintz, D. Forster, D.E. Morris, Inorganic Synthesis, vol. 28, Wiley, New York, 1991, p. 88.
37. Boullanger, S.; Contal, E.; Buron, C. C.; Viau, L., Pyrrole-tailed imidazolium surface-active monomers: aggregation properties in aqueous solution and polymerization behavior. *J. Mol. Liq.* **2022,** *350*, 118588.
38. Beillard, A.; Golliard, E.; Gillet, V.; Bantreil, X.; Métro, T.-X.; Martinez, J.; Lamaty, F., Expedient Mechanosynthesis of *N,N*-Dialkyl Imidazoliums and Silver(I)–Carbene Complexes in a Ball-Mill. *Chem. Eur. J.* **2015,** *21* (49), 17614-17617.
39. Wang, H. M. J.; Lin, I. J. B., Facile Synthesis of Silver(I)−Carbene Complexes. Useful Carbene Transfer Agents. *Organometallics* **1998,** *17* (5), 972-975.
40. de Frémont, P.; Scott, N. M.; Stevens, E. D.; Nolan, S. P., Synthesis and Structural Characterization of *N*-Heterocyclic Carbene Gold(I) Complexes. *Organometallics* **2005,** *24* (10), 2411-2418.
41. Viau, L.; Hihn, J. Y.; Lakard, S.; Moutarlier, V.; Flaud, V.; Lakard, B., Full Characterization of Polypyrrole Thin Films Electrosynthesized in Room Temperature Ionic Liquids, Water or Acetonitrile. *Electrochim. Acta* **2014,** *137*, 298-310.
42. Sadki, S.; Schottland, P.; Brodie, N.; Sabouraud, G., The Mechanisms of Pyrrole Electropolymerization. *Chem. Soc. Rev.* **2000,** *29* (5), 283-293.
43. Zhou, M.; Heinze, J., Electropolymerization of Pyrrole and Electrochemical Study of Polypyrrole. 3. Nature of "Water Effect" in Acetonitrile. *J. Phys. Chem. B* **1999,** *103* (40), 8451-8457.
44. Carquigny, S.; Lakard, B.; Lakard, S.; Moutarlier, V.; Hihn, J.-Y.; Viau, L., Investigation of Pharmaceutically Active Ionic Liquids as Electrolyte for the Electrosynthesis of Polypyrrole and Active Component in Controlled Drug Delivery. *Electrochim. Acta* **2016,** *211*, 950-961.
45. da Silva Jr, F. A. G.; Queiroz, J. C.; Macedo, E. R.; Fernandes, A. W. C.; Freire, N. B.; da Costa, M. M.; de Oliveira, H. P., Antibacterial behavior of polypyrrole: The influence of morphology and additives incorporation. *Mater. Sci. Eng., C* **2016,** *62*, 317-322.
46. Chen, X.; Issi, J.-P.; Devaux, J.; Billaud, D., Chemically Oxidized Polypyrrole: Influence of the Experimental Conditions on its Electrical Conductivity and Morphology. *Polym. Eng. Sci.* **1995,** *35* (8), 642-647.
47. Carquigny, S.; Segut, O.; Lakard, B.; Lallemand, F.; Fievet, P., Effect of Electrolyte Solvent on the Morphology of Polypyrrole Films: Application to the Use of Polypyrrole in pH Sensors. *Synth. Met.* **2008,** *158* (11), 453-461.

48. Ge, H.; Qi, G.; Kang, E.-T.; Neoh, K. G., Study of Overoxidized Polypyrrole Using X-ray Photoelectron Spectroscopy. *Polymer* **1994,** *35* (3), 504-508.
49. Jaramillo, A.; D. Spurlock, L.; Young, V.; Brajter-Toth, A., XPS Characterization of Nanosized Overoxidized Polypyrrole Films on Graphite Electrodes. *Analyst* **1999,** *124* (8), 1215-1221.
50. Zhang, Z.; Gao, H.; Wu, H.; Qian, Y.; Chen, L.; Chen, J., Chemical Fixation of CO_2 by Using Carbon Material-Grafted N-Heterocyclic Carbene Silver and Copper Complexes. *ACS Appl. Nano Mater.* **2018,** *1* (11), 6463-6476.
51. Pažický, M.; Loos, A.; Ferreira, M. J.; Serra, D.; Vinokurov, N.; Rominger, F.; Jäkel, C.; Hashmi, A. S. K.; Limbach, M., Synthesis, Reactivity, and Electrochemical Studies of Gold(I) and Gold(III) Complexes Supported by *N*-Heterocyclic Carbenes and Their Application in Catalysis. *Organometallics* **2010,** *29* (20), 4448-4458.
52. Au, V. K.-M.; Wong, K. M.-C.; Zhu, N.; Yam, V. W.-W., Luminescent Cyclometalated *N*-Heterocyclic Carbene-Containing Organogold(III) Complexes: Synthesis, Characterization, Electrochemistry, and Photophysical Studies. *J. Am. Chem. Soc.* **2009,** *131* (25), 9076-9085.
53. Süzer, Ş., XPS Investigation of X-Ray-Induced Reduction of Metal Ions. *Appl. Spectrosc.* **2000,** *54* (11), 1716-1718.
54. Kluson, P.; Krystynik, P.; Dytrych, P.; Bartek, L., Interactions of the (R) Ru-BINAP Catalytic Complex with an Inorganic Matrix in Stereoselective Hydrogenation of Methylacetoacetate: Kinetic, XPS and DRIFT Studies. *Reac. Kinet. Mech. Cat.* **2016,** *119* (2), 393-413.
55. Wang, R.; Qin, L.; Wang, X.; Chen, B.; Zhao, Y.; Gao, G., Polymer Supported *N*-Heterocyclic Carbene Ruthenium Complex Catalyzed Transfer Hydrogenation of Ketones. *Catal. Commun.* **2020,** *138*, 105924.
56. Biesinger, M. C.; Lau, L. W. M.; Gerson, A. R.; Smart, R. S. C., Resolving Surface Chemical States in XPS Analysis of First Row Transition Metals, Oxides and Hydroxides: Sc, Ti, V, Cu and Zn. *Appl. Surf. Sci.* **2010,** *257* (3), 887-898.
57. Schmidt, C.; Karge, B.; Misgeld, R.; Prokop, A.; Franke, R.; Brönstrup, M.; Ott, I., Gold(I) NHC Complexes: Antiproliferative Activity, Cellular Uptake, Inhibition of Mammalian and Bacterial Thioredoxin Reductases, and Gram-Positive Directed Antibacterial Effects. *Chem. Eur. J.* **2017,** *23* (8), 1869-1880.
58. Ceramella, J.; Troiano, R.; Iacopetta, D.; Mariconda, A.; Pellegrino, M.; Catalano, A.; Saturnino, C.; Aquaro, S.; Sinicropi, M. S.; Longo, P., Synthesis of Novel *N*-

Heterocyclic Carbene-Ruthenium (II) Complexes, “Precious” Tools with Antibacterial, Anticancer and Antioxidant Properties. *Antibiotics* **2023,** *12* (4), 693.

59. Boubakri, L.; Chakchouk-Mtibaa, A.; Al-Ayed, A. S.; Mansour, L.; Abutaha, N.; Harrath, A. H.; Mellouli, L.; Özdemir, I.; Yasar, S.; Hamdi, N., Ru(II)–*N*-Heterocyclic Carbene Complexes: Synthesis, Characterization, Transfer Hydrogenation Reactions and Biological Determination. *RSC Adv.* **2019,** *9* (59), 34406-34420.

60. Pan, T.; Wang, Y.; Liu, F.-S.; Lin, H.; Zhou, Y., Copper(I)–NHCs Complexes: Synthesis, Characterization and Their Inhibition Against the Biofilm Formation of Streptococcus Mutans. *Polyhedron* **2021,** *197*, 115033.

61. Sarı, Y.; Akkoç, S.; Gök, Y.; Sifniotis, V.; Özdemir, İ.; Günal, S.; Kayser, V., Benzimidazolium-Based Novel Silver N-Heterocyclic Carbene Complexes: Synthesis, Characterisation and In Vitro Antimicrobial Activity. *J. Enzyme Inhib. Med. Chem.* **2016,** *31* (6), 1527-1530.

62. Yıldırım, I.; Aktaş, A.; Celepci, D. B.; Kırbağ, S.; Kutlu, T.; Gök, Y.; Aygün, M., Synthesis, Characterization, Crystal Structure, and Antimicrobial Studies of 2-Morpholinoethyl-Substituted Benzimidazolium Salts and Their Silver(I)-*N*-Heterocyclic Carbene Complexes. *Res. Chem. Intermed.* **2017,** *43* (11), 6379-6393.

63. Aher, S.; Das, A.; Muskawar, P.; Osborne, J.; Bhagat, P., Synthesis, Characterization and Antimicrobial properties of Methylbenzyl and Nitrobenzyl containing Imidazolium-based Silver *N*-Heterocyclic Carbenes. *J. Mol. Liq.* **2017,** *233*, 270-277.

64. Kaloğlu, N.; Özdemir, İ.; Günal, S.; Özdemir, İ., Synthesis and Antimicrobial Activity of Bulky 3,5-Di-Tert-Butyl Substituent-Containing Silver–*N*-Heterocyclic Carbene Complexes. *Appl. Organomet. Chem.* **2017,** *31* (11), e3803.

65. Cui, S.; Mao, J.; Rouabhia, M.; Elkoun, S.; Zhang, Z., A Biocompatible Polypyrrole Membrane for Biomedical Applications. *RSC Adv.* **2021,** *11* (28), 16996-17006.

66. Zhang, X.; Wang, S.; Tang, K.; Pan, W.; Xu, H.; Li, Y.; Gao, Y.; Li, N.; Tang, B., Cu2+ Embedded Three-Dimensional Covalent Organic Framework for Multiple ROS-Based Cancer Immunotherapy. *ACS Appl. Mater. Interfaces* **2022,** *14* (27), 30618-30625.

67. Dianatdar, A.; Miola, M.; De Luca, O.; Rudolf, P.; Picchioni, F.; Bose, R. K., All-Dry, One-Step Synthesis, Doping and Film Formation of Conductive Polypyrrole. *J. Mater. Chem. C* **2022,** *10* (2), 557-570.

68. Forest, V.; Figarol, A.; Boudard, D.; Cottier, M.; Grosseau, P.; Pourchez, J., Adsorption of Lactate Dehydrogenase Enzyme on Carbon Nanotubes: How to Get Accurate Results for the Cytotoxicity of These Nanomaterials. *Langmuir* **2015,** *31* (12), 3635-3643.

69. Adhikari, S.; Nath, P.; Das, A.; Datta, A.; Baildya, N.; Duttaroy, A. K.; Pathak, S., A Review on Metal Complexes and Its Anti-Cancer Activities: Recent Updates from In Vivo Studies. *Biomed. Pharmacother.* **2024,** *171*, 116211.
70. Visbal, R.; Fernández-Moreira, V.; Marzo, I.; Laguna, A.; Gimeno, M. C., Cytotoxicity and Biodistribution Studies of Luminescent Au(i) and Ag(i) *N*-Heterocyclic Carbenes. Searching for New Biological Targets. *Dalton Trans.* **2016,** *45* (38), 15026-15033.
71. Dabiri, Y.; Schmid, A.; Theobald, J.; Blagojevic, B.; Streciwilk, W.; Ott, I.; Wölfl, S.; Cheng, X., A Ruthenium(II) *N*-Heterocyclic Carbene (NHC) Complex with Naphthalimide Ligand Triggers Apoptosis in Colorectal Cancer Cells via Activating the ROS-p38 MAPK Pathway. *Int. J. Mol. Sci.* **2018,** *19* (12), 3964.

For Table of Content Only